International Journal of Design & Nature and Ecodynamics
Vol. 19, No. 4, August, 2024, pp. 1231-1242
Journal homepage: http://iieta.org/journals/ijdne

Sediment Transport of Cohesive Sediment in Kanal Banjir Barat Jakarta Using Non-Orthogonal Boundary Fitted Model

Denny Yatmadi[1,2*], Muhammad Syahril Badri Kusuma[3], Muslim Muin[4], Nita Yuanita[4], Arung Bahari Muslim[5], Heru Nur Alam[5]

[1] Doctoral Program of Civil Engineering, Faculty of Civil and Environmental Engineering, Institut Teknologi Bandung, Bandung 40132, Indonesia
[2] Department of Civil Engineering, Politeknik Negeri Jakarta, Depok 16425, Indonesia
[3] Water Resources Engineering Research Group, Faculty of Civil and Environmental Engineering, Institut Teknologi Bandung, Bandung 40132, Indonesia
[4] Coastal Engineering Research Group, Faculty of Civil and Environmental Engineering, Institut Teknologi Bandung, Bandung 40132, Indonesia
[5] MuTeknologi Software, Bandung 40124, Indonesia

Corresponding Author Email: denny.yatmadi@gmail.com

https://doi.org/10.18280/ijdne.190414

Received: 30 April 2024
Revised: 12 July 2024
Accepted: 18 July 2024
Available online: 28 August 2024

Keywords:
cohesive sediment, critical shear stress, settling velocity, Non-Orthogonal Boundary Fitted, Kanal Banjir Barat, sediment transport, numerical model

ABSTRACT

The Kanal Banjir Barat (KBB) located in Jakarta crosses seven kilometers from Season City Jakarta to Kali Adem Estuary in the north of Jakarta, which is dominated by the organic with the median diameter of cohesive sediment ranges from 0.001 to 0.01mm. As an artificial channel through which river water travels from upstream to downstream of the sea, the Kanal Banjir Barat must be preserved to prevent sedimentation from reducing its width and depth. This research aims to present an analysis of cohesive sediment simulation using a numerical model and present the sedimentation deposition using the Non-Orthogonal Boundary Fitted (NOBF) model. Important parameters such as critical shear stress and settling velocity are also considered in this model. The best value for friction coefficient after trial and error for calibration is 0.001, resulting in a Root Mean Square Error (RMSE) for the water level of 0.0373 and 0.02 with Nash-Sutcliffe Efficiency (NSE) of 0.45 and 0.55, respectively. Based on the findings from the calibration and validation processes in both dry and wet seasons, it is evident that the models show good comparisons with field observation data. Model deposition simulation with excellent simulation results will run for four years, from December 2022 until December 2026.

1. INTRODUCTION

The Kanal Banjir Barat (KBB), located in Jakarta, crosses 7 kilometers from Season City to the Kali Adem estuary north of Jakarta. The distribution of cohesive sedimentation along the KBB originates from the upstream KBB and is influenced by four rivers along the KBB. From laboratory tests and refer to USCS soil classification [1], the soil of this location is dominated by MH/OH type with a 20-40% Plasticity Index value, and the median diameter of cohesive sediment ranges from 0.001 to 0.01mm. Understanding the sedimentation process in rivers is important to sustain water in terms of quantity and quality while minimizing the risks that emerge due to cohesive sediment sedimentation.

Currently, there has not been research that demonstrated related sedimentation in Banjir Kanal Barat. Previous studies at this research location, Kanal Banjir Barat (KBB), have always concentrated on flooding, not sedimentation, especially cohesive sediments. Kanal Banjir Barat has vital functions as an artificial channel to accommodate four rivers as well as anticipate flooding in the middle and downstream areas of Jakarta.

KBB, located downstream in the river and flows into the estuary, is predominately composed of cohesive, fine-grained sediments transported downstream from their source upland. Density Induced Current in river streams in which seawater infiltrates, current processes facilitate the aggregation of fine-grained cohesive sediments by saltwater, which subsequently settle in specific sections of the river, particularly in the zone where freshwater and saltwater converge due to the transport of seawater during high tides. As an artificial channel through which river water travels from upstream to downstream of the sea, the Kanal Banjir Barat must be preserved to prevent sedimentation from reducing its width and depth.

The deposition of sediment present in a given section of a river stream significantly impacts the river's downstream flow to the sea. Consequently, it is important to conduct research concerning cohesive sediment movement, with a particular focus on the mixed zone region, where salinity and tides influence sediment deposition.

A primary focus in improving numerical modeling and conceptual understanding of fine sediment dynamics has been correctly estimating fall velocity (FV), a vital metric for sediment researchers [2]. Previous research has shown both measured and predicted settling velocities (cm/s) as a function of sediment size [3].

The Sediment Concentration Input (SSC) that utilizes the pre-limitation also contributes to the model's performance, but only in modeling flood occurrences. It has been discovered that it impacts the process of dispersing adjectives, although its effect on erosion sedimentation is not very substantial [4]. Coastal ecosystem wellness is determined by the amount and the quality of suspended sediments transported by runoff from the land to the river [5].

Complex modeling issues can be partly assisted by numerical modeling, particularly in hydrodynamics. The water level of Katulampa Barrage is predicted in this study utilizing Long Short-Term Memory (LSTM) Recurrent Neural Networks (RNN) and Sadewa data [6]. Researchers used a hydrodynamic model that considers river and estuary sediment transport to compile their findings [7]. The research region in Palembang effectively characterizes the hydrodynamic state in the fluvial-estuarine transition area by comparing model outputs with measurement data during the validation and verification phase [8]. Using a hybrid of the Mc Cormack and splitting techniques, the numerical model's application was built using the finite difference approach to solve the hydrodynamic problem [9].

A suspended sediment movement module was incorporated into a three-dimensional, unstructured-grid hydrodynamic model of the Danshui River, which corresponded substantially with the measurements [10]. The Klarälven River in southwestern Sweden was analyzed using a three-dimensional flow model that included the RNG k-turbulence model and a non-equilibrium wall function. This research examined the Klarälven River using a three-dimensional flow model that included the RNG k-turbulence model and a non-equilibrium wall function [11]. Numerical models may be used to analyze probable tsunami risks in the Palu area in central Sulawesi [12]. A new model was developed that can analyze the effects of horizontal convective transport, and a vertically suspended upward movement on the SSC, and show good results between the model and observation at the Yangtze River Estuarine [13].

This research aims to simulate sedimentation deposition at KBB using data from the field and model simulations. Furthermore, from the results of this model simulation, the next steps related to the impact of sedimentation at the study location can be determined. Prior research has been carried out at the same site, focusing only on flood-related effects [14].

The study employs a 3D Ocean Hydrodynamics model and Sediment Transport Model called MuSed3D. A model that can accommodate these conditions is necessary due to the complicated geometry of the existing KBB river. The MuSed 3D model was selected due to its compliance with these criteria. The model utilizes Muin's Non-Orthogonal boundary-fitted technique [15]. The application of the model to the Providence River demonstrates its capability to accurately forecast the flow patterns in an estuary with intricate geometry and bathymetry. The model demonstrates the significance of bed friction in regulating flow parameters in this area [16]. This design has been implemented extensively in Indonesia and internationally, including the San Fransico Bay [17], the Bay of Fundy [18].

2. MATERIAL AND METHOD

2.1 Location of study

The study site is at the Kanal Banjir Barat (KBB), north of Jakarta, Indonesia. It is a part of the Ciliwung River in its upper reaches and is bounded by the Manggarai watergate. This KBB starts from South to North with approximately 16km, the upstream part is the Manggarai sluice gate located in the South Jakarta area (-6.2080; 106.8481) and the downstream part is the estuary located in the North Jakarta area with coordinates (-6.1037; 106.7674). The study location concentrates on just part of the rivers close that are influenced by salinity and tides, particularly a 7-kilometer length between Season City bridge to Kali Adem estuary, displayed in Figure 1.

The Kanal Banjir Barat is an artificial canal having functions to accommodate four rivers in Jakarta, namely the Angke River, Krukut River, Cideng River, and Grogol River. KBB has a width of 30 meters in the upstream section, 50 meters in the middle section, and 65 meters in the downstream section [19].

2.2 Data availability

This study uses three types of data: calibration, validation, and simulation. The 30-day water level elevation measurements collected from the Sunda Kelapa station in August 2023 and the 8-day water level elevation measurements collected from Kali Adem estuary in May 2023 provide the data used for calibration.

On the other hand, the data used for validation, comes from two separate sites where sediment concentration was tested in the field in August 2023. Using data from the Karet Watergate, the simulation model accounts from Early 2023 until Late 2026.

2.3 Model description

In preparation for utilizing a hydrodynamic model that exhibits significant differences in latitude, Spaulding devised a boundary-fitted spherical coordinate model and resolved the vertically averaged equations of motion using Leendertse's [20] multi-operational approach in curvilinear coordinates.

The model was further enhanced by Swanson et al. [21] and Muin and Spaulding [22] by converting both the dependent variables (the velocity components) and the independent variables (coordinate geometry) into curvilinear coordinates. A three-dimensional solution was introduced using a split technique, which divides the governing equations into an exterior mode (vertically averaged) and an interior mode (vertical structure).

The conceptual basis of the model is established by the continuity and momentum equations. Both equations were derived under the assumption that the flow is incompressible, except for negligible variation in water mass density when multiplied by the earth's gravity (Boussinesq approximation), and the neglect of vertical acceleration compared to gravitational acceleration (hydrostatic approximation).

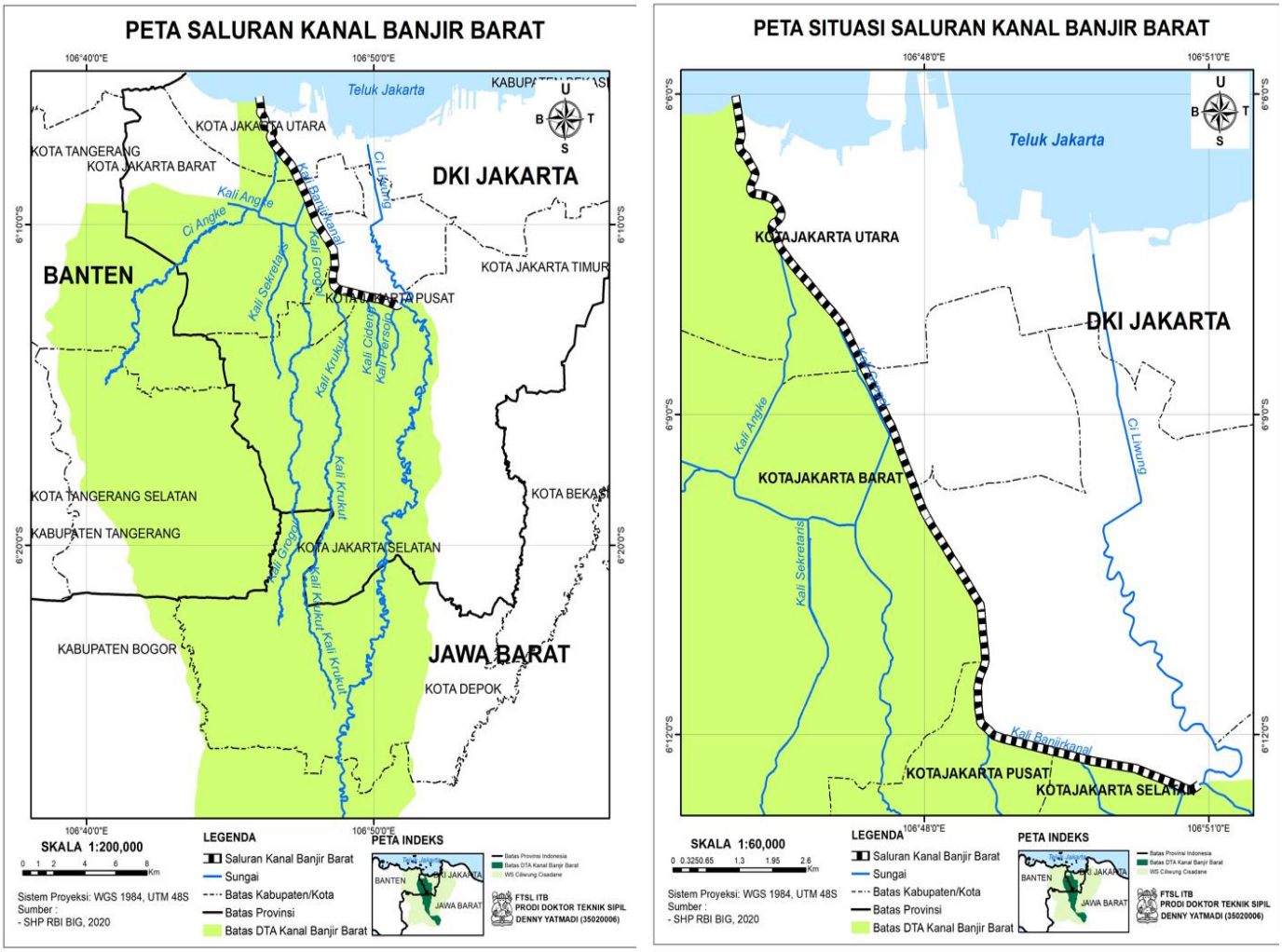

Figure 1. Location of study

The beach is considered an impermeable surface along the shoreline, meaning that there is no fluid particle velocity perpendicular to it. The boundary condition on the ocean side is determined by the time-varying water surface elevation. River inflows can be accounted for by determining their discharge. There are two choices for specifying shear stresses at the bottom: (1) Quadratic stress law or (2) Manning coefficient. The wind stress at the free surface is determined using a quadratic approximation. To do calculations in a curvilinear system with a mesh composed of square grids, the dependent and independent variables in Eqs. (1) until (3) mentioned below are converted into a curvilinear coordinate system.

Continuity equation

$$Jr\cos\theta\frac{\partial\zeta}{\partial t}+\frac{\partial}{\partial\xi}\left(\cos\theta Ju^cD\right)+\frac{\partial}{\partial\eta}\left(\cos\theta Jv^cD\right)+Jr\cos\theta\frac{\partial(\omega D)}{\partial\sigma}=0 \quad (1)$$

Momentum equation

- **ξ-direction**

$$\begin{aligned}\frac{\partial u^cD}{\partial t}=&-\frac{\theta_\eta\theta_\eta+\cos^2\theta\,\varphi_\eta\varphi_\eta}{J^2\rho_0 r\cos^2\theta}\frac{Dg}{2}\Big[\{\lambda\\&+(\rho_s-2\rho)(1-\sigma)\}\frac{\partial D}{\partial\zeta}\\&+(4\rho-2\rho_s)\frac{\partial\zeta}{\partial\zeta}+D\frac{\partial\lambda}{\partial\zeta}\Big]\\&+\frac{\theta_\zeta\theta_\eta+\cos^2\theta\,\varphi_\zeta\varphi_\eta}{J^2\rho_0 r\cos^2\theta}\frac{Dg}{2}\Big[\{\lambda+(\rho_s-2\rho)(1-\sigma)\}\frac{\partial D}{\partial\eta}\\&+(4\rho-2\rho_s)\frac{\partial\zeta}{\partial\eta}+D\frac{\partial\lambda}{\partial\eta}\Big]\\&-\frac{\theta_\eta}{J^2r\cos^2\theta}\left[\begin{matrix}\frac{\partial}{\partial\zeta}\left(\varphi_\zeta\cos^2\theta\,Ju^cu^cD+\varphi_\eta\cos^2\theta\,Ju^cv^cD\right)\\+\frac{\partial}{\partial_\eta}\left(\varphi_\zeta\cos^2\theta\,Ju^cv^cD+\varphi_\eta\cos^2\theta\,Jv^cv^cD\right)\end{matrix}\right]\\&+\frac{\varphi_\eta}{J^2r\cos^2\theta}\left[\begin{matrix}\frac{\partial}{\partial\zeta}\left(\theta_\zeta\cos^2\theta\,Ju^cu^cD+\theta_\eta\cos^2\theta\,Ju^cv^cD\right)\\+\frac{\partial}{\partial\eta}\left(\theta_\zeta\cos^2\theta\,Ju^cv^cD+\theta_\eta\cos^2\theta\,Jv^cv^cD\right)\end{matrix}\right]\\&-\frac{\partial}{\partial\sigma}(\omega u^cD)+\frac{fD}{J\cos\theta}\left[\begin{matrix}(\theta_\zeta\theta_\eta+\cos^2\theta\,\varphi_\zeta\varphi_\eta)u_c\\+(\theta_\eta\theta_\eta+\cos^2\theta\,\varphi_\eta\varphi_\eta)v^c\end{matrix}\right]\\&+\frac{4}{D}\frac{\partial}{\partial\sigma}\left(A_v\frac{\partial u^c}{\partial\sigma}\right)\end{aligned} \quad (2)$$

- **η-direction**

$$\frac{\partial v^c D}{\partial t} = \frac{\theta_\eta \theta_\xi + \cos^2\theta\,\varphi_\eta\varphi_\xi}{J^2\rho_0 r\cos^2\theta}\frac{Dg}{2}\left[\{\lambda + (\rho_s - 2\rho)(1 - \sigma)\}\frac{\partial D}{\partial \xi} + (4\rho - 2\rho_s)\frac{\partial \zeta}{\partial \xi} + D\frac{\partial \lambda}{\partial \xi}\right]$$
$$- \frac{\theta_\xi \theta_\xi + \cos^2\theta\,\varphi_\xi\varphi_\xi}{J^2\rho_0 r\cos^2\theta}\frac{Dg}{2}\left[\{\lambda + (\rho_s - 2\rho)(1 - \sigma)\}\frac{\partial D}{\partial \eta} + (4\rho - 2\rho_s)\frac{\partial \zeta}{\partial \eta} + D\frac{\partial \lambda}{\partial \eta}\right]$$
$$+ \frac{\theta_\xi}{J^2 r\cos^2\theta}\left[\begin{matrix}\frac{\partial}{\partial \xi}\left(\varphi_\xi \cos^2\theta\, J u^c u^c D + \varphi_\eta \cos^2\theta\, J u^c v^c D\right) \\ + \frac{\partial}{\partial \eta}\left(\varphi_\xi \cos^2\theta\, J u^c v^c D + \varphi_\eta \cos^2\theta\, J v^c v^c D\right)\end{matrix}\right] \quad (3)$$
$$- \frac{\varphi_\xi}{J^2 r\cos^2\theta}\left[\begin{matrix}\frac{\partial}{\partial \xi}\left(\theta_\xi \cos^2\theta\, J u^c u^c D + \theta_\eta \cos^2\theta\, J u^c v^c D\right) \\ + \frac{\partial}{\partial \eta}\left(\theta_\xi \cos^2\theta\, J u^c v^c D + \theta_\eta \cos^2\theta\, J v^c v^c D\right)\end{matrix}\right]$$
$$- \frac{\partial}{\partial \sigma}(\omega v^c D) - \frac{fD}{J\cos\theta}\left[\left(\theta_\xi\theta_\xi + \cos^2\theta\,\varphi_\xi\varphi_\xi\right)u_c + \left(\theta_\xi\theta_\eta + \cos^2\theta\,\varphi_\xi\varphi_\eta\right)v^c\right]$$
$$+ \frac{4}{D}\frac{\partial}{\partial \sigma}\left(A_v\frac{\partial v^c}{\partial \sigma}\right)$$

Furthermore, the inclusion of sediment, salinity, and temperature necessitates the consideration of both the equation for conservation of substance and the equation of state. The equations are shown in Eqs. (4) and (5).

$$\frac{\partial q}{\partial t} + \frac{u^c}{r}\frac{\partial q}{\partial \xi} + \frac{v^c}{r}\frac{\partial q}{\partial \eta} + \omega\frac{\partial q}{\partial \sigma} = \frac{4}{D^2}\frac{\partial}{\partial \sigma}\left(D_v\frac{\partial q}{\partial \sigma}\right)$$
$$+ \frac{D_h}{r^2 J^2}\left[\begin{matrix}\left(\frac{\theta_\eta\theta_\eta}{\cos^2\theta} + \varphi_\eta\varphi_\eta\right)\frac{\partial^2 q}{\partial \xi^2} - 2\left(\frac{\theta_\xi\theta_\eta}{\cos^2\theta} + \varphi_\xi\varphi_\eta\right)\frac{\partial^2 q}{\partial \xi\partial \eta} \\ + \left(\frac{\theta_\xi\theta_\xi}{\cos^2\theta} + \varphi_\xi\varphi_\xi\right)\frac{\partial^2 q}{\partial \eta^2}\end{matrix}\right] \quad (4)$$

The above governing equations are solved numerically using a semi-implicit technique where the water surface elevation in the long wave equation is solved implicitly and the other variables explicitly. By adopting this combination, the time-step size in the numerical solution is not constrained by the shallow water wave celerity, hence facilitating rapid computer execution.

2.4 Model numerical preparation

The study employs a 3D Ocean Hydrodynamics and sediment transport model called MuSed3D. MuSed3D utilizes Muin's Non-Orthogonal boundary-fitted technique in spherical coordinates [15]. MuSed3D features multiple essediment classes and cohesive and noncohesivesediment for the sediment transport simulation. MuSed3D is also embedded with a Geographic Information System (GIS) to simplify the user to understand the simulation results. The hydrodynamic model has been implemented extensively in Indonesia and internationally, including the Providence River [16], San Fransico Bay [17], and the Bay of Fundy [18]. The sedimentation results have been applied in Indonesia such as studies [23-26]. In terms of modeling, two crucial steps will be taken to achieve the best outcomes: the first is the model calibration step, which involves making adjustments through trial and error until the model's output matches the observations. The validation stage, which involves comparing the model findings with the observation results, comes next. In the calibration phase, the model's water elevation from two locations outputs will be compared to observations collected over seven days from 14 to 22 May, 2023, and 30 days from August 2023. In the meantime, during the validation phase, the outcomes of the observations conducted in August 2023 for sediment concentration were compared with the results of the model sediment concentration values.

Parameter setting

Before the analysis, crucial components of the model setup, including the modeling parameters, must be ready. Seabed friction, Critical shear stress, physical characteristics of sediment, water elevation, river components, and sediment density are the parameters that are under consideration. The model preparation parameters are listed in Table 1.

Table 1. Set up parameters for a model

Parameter	Value	Unit
Critical shear stress for erosion	1.0	Pa
Critical shear stress for deposition	0.5	Pa
Settling velocity	0.8	$mm.s^{-1}$
Friction coefficient	0.001	
Density sediment	1600	$Kg.m^{-3}$

Critical shear stress

Critical shear stress (τ_c) is the threshold condition of shear stress obtained from flowing water just before soil erosion occurs [27]. According to Nafchi et al. [28], the τ_c* of the mudstone deposits varied between 0.13 and 1.4 Pa and was set at 1.0 shear stress for erosion and 0.5 for shear stress for deposition.

Density sediment

From the results of laboratory tests and based on the USCS classification system, it can be concluded that the soil type at the research location is MH/OH or inorganic silt with medium to high plasticity with a Density of $1600 Kg.m^{-3}$.

Settling velocity

The settling velocity of particulate sediment in Papua Indonesia was determined using an empirical formula derived from a laboratory experiment by Muin [24] will be implemented for this model. The formula has been applied to several places in Indonesia such as Bintuni [24], Port of Kuala Tanjung [23] and many more places.

Friction coefficient

The friction coefficient values at the base of the model were calibrated by an iterative process of trial and error. This process led to the determination of the best value of 0.001.

3. NUMERICAL MODEL

3.1 Grid system

This model uses a non-orthogonal grid system and bathymetric data from Dishidros DKI [29]. Proposed grids are closer to the location of interest compared to areas further away from the study location and using non-uniform sizes. The size of the grid in the river is smaller than the grid in the sea. This scenario implies avoiding of influence of open boundaries on the study location (river). Figure 2 is a grid system model with Non Orthogonal Boundary Fitted (NOBF) that will implemented for this study.

Figure 2. Grid system NOBF model

3.2 Governing equation

The governing equation of suspended sediment can be written as follows:

$$\frac{\partial \Omega^n}{\partial t}+\frac{u^c}{r}\frac{\partial \Omega^n}{\partial \xi}+\frac{v^c}{r}\frac{\partial \Omega^n}{\partial \eta}+(\omega-\omega^n{}_s)\frac{\partial \Omega^n}{\partial \sigma}= \frac{4}{D^2}\frac{\partial}{\partial \sigma}\left(D_v\frac{\partial \Omega^n}{\partial \sigma}\right) + \frac{D_h}{r^2J^2}\left[\left(\frac{\theta_\eta\theta_\eta}{cos^2\theta}+\varphi_\eta\varphi_\eta\right)\frac{\partial^2\Omega^n}{\partial\xi^2}-2\left(\frac{\theta_\xi\theta_\eta}{cos^2\theta}+\varphi_\xi\varphi_\eta\right)\frac{\partial^2\Omega^n}{\partial\xi\partial\eta} + \left(\frac{\theta_\xi\theta_\xi}{cos^2\theta}+\varphi_\xi\varphi_\xi\right)\frac{\partial^2\Omega^n}{\partial\eta^2}\right] + Erosion \quad (5)$$

The governing equations of deposit sediment can be written as follows:

$$\frac{dm_d}{dt}=\omega_s C\left(1-\frac{\sigma_b}{\sigma_d}\right) \text{ for } \frac{\sigma_b}{\sigma_d}<1 \quad (6)$$

$$\frac{dm_d}{dt}=0 \text{ for } \frac{\sigma_b}{\sigma_d}>1 \quad (7)$$

where, $\frac{dm_d}{dt}$ is deposit sediment, C is Sediment concentration (ppm), σ_b is bottom-shear stress (pa), σ_d is Critical shear stress for deposit sediment (pa), ω_s is settling velocity (m/s).

The governing equation of erosion can be written as follows:

$$\text{Erosion}=E_0\left(\left(\frac{\sigma_b}{\sigma_e}\right)^k-1\right)\frac{\rho_s}{h_{cell}} for \frac{\sigma_b}{\sigma_e}>1 \quad (8)$$

4. RESULT AND DISCUSSION

4.1 Model calibration

Adjustments were made to these calibration parameters via trial and error to get the best possible outcome. It was necessary to do calibration to get the most accurate findings for the friction coefficient. This study will use water level and current speed measurements conducted in May 2023 and August 2023, respectively, at Kali Adem Estuary and STA Sunda Kelapa, for the calibration hydrodynamic model, as shown in Figure 3. In this research, the friction coefficient will be iteratively adjusted via trial and error until an ideal outcome is achieved, which will then be compared with the observed data. An iterative process of trial and error calibrated the friction coefficient values at the model's base. This process led to the determination of the best value of 0.001. Figure 4 shows the calibration results for water elevation between the model and observation at Kali Adem Estuary, resulting in a root mean square error (RMSE) of 0.0373 and Nash-Sutcliffe Efficiency (NSE) of 0.45, Figure 5 shows the calibration results for water elevation between the model and observation at STA Sunda Kelapa with resulting in a root mean square error (RMSE) of 0.02 and Nash-Sutcliffe Efficiency (NSE) of 0.55.

On 7 August 2023, measurement of the water height and the current speed per second at two separate sites, the Kali Adem Estuary and Sunda Kelapa served as calibration parameters.

Figure 6 shows the calibration results for the current speed between the model and observation at Kali Adem Estuary, Figure 7 shows the calibration results for the current speed between the model and observation at STA Sunda Kelapa with a lower of less than 10% from the model.

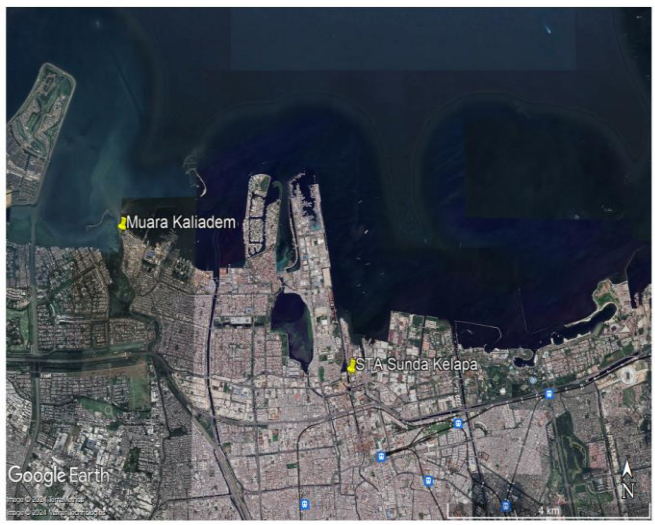

Figure 3. Location for calibration (Google Earth)

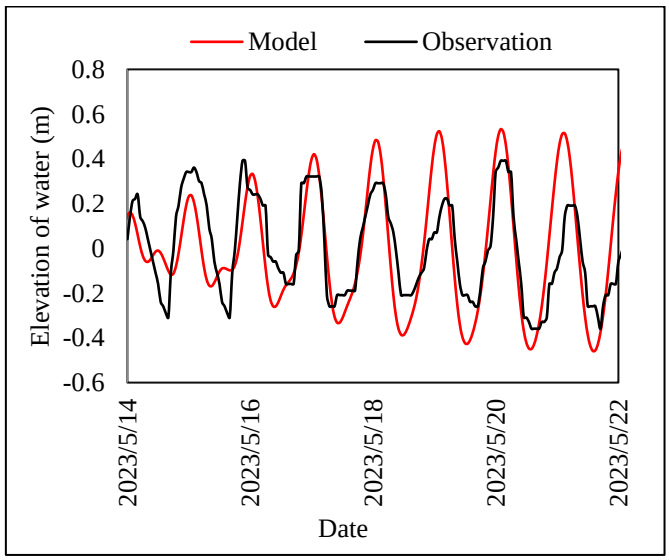

Figure 4. Calibration model for water elevation at Muara Kaliadem

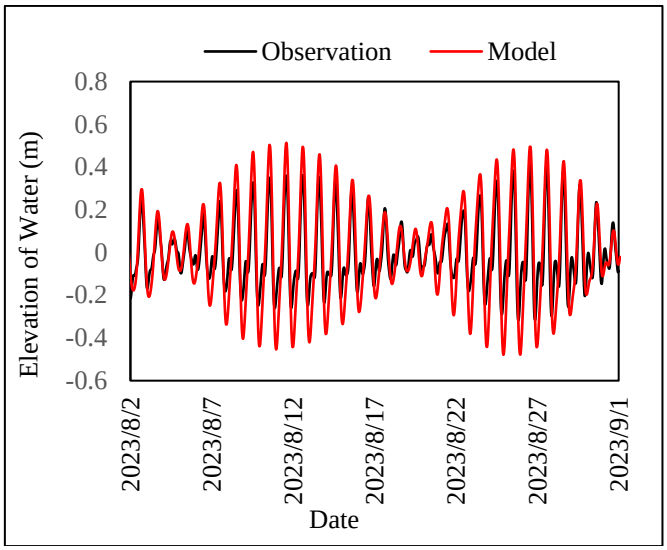

Figure 5. Calibration model for water elevation at STA. Sunda Kelapa

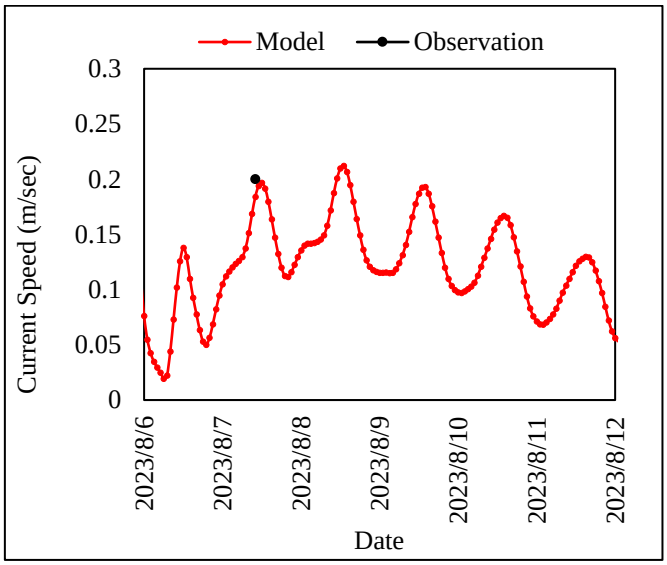

Figure 6. Calibration model for current speed at Kaliadem estuary

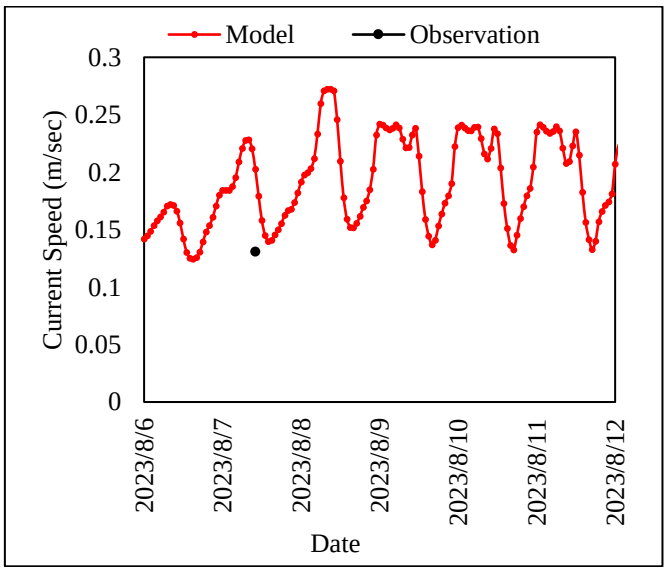

Figure 7. Calibration model for current speed at STA. Sunda Kelapa

4.2 Model validation

Measured sediment concentration (SSC) at two locations will be used for the model's validation. To ensure accuracy, the modeling results for suspended sediment concentrations were cross-checked with observed data from August 2023 during the dry season and December 2022 during the wet season . For validation purposes, the physical parameter for bed friction coefficient is 0.001; the erosion rate is 0.2 mm/hour; simulation starts from 1 August 2023 for 40 days; the physical parameter for sediment settling velocity is 0.8 mm/s; critical shear stress for erosion 1.0 Pa; critical shear stress for deposition 0.5 Pa; density sediment 1600Kg.m^{-3}. SSC location for validation purposes is presented in Figure 8 below.

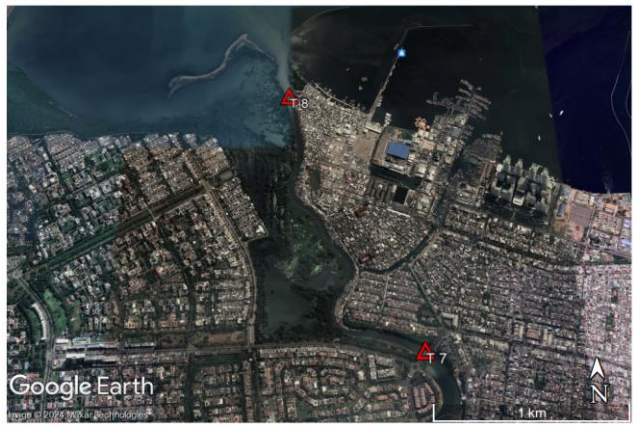

Figure 8. Location for validation model (Google Earth)

The sediment concentration measurements at two separate sites will validate the consistency between the model and the real-world conditions. At each location, there was a satisfactory agreement between the model and observed values of the suspended sediment concentration distribution.

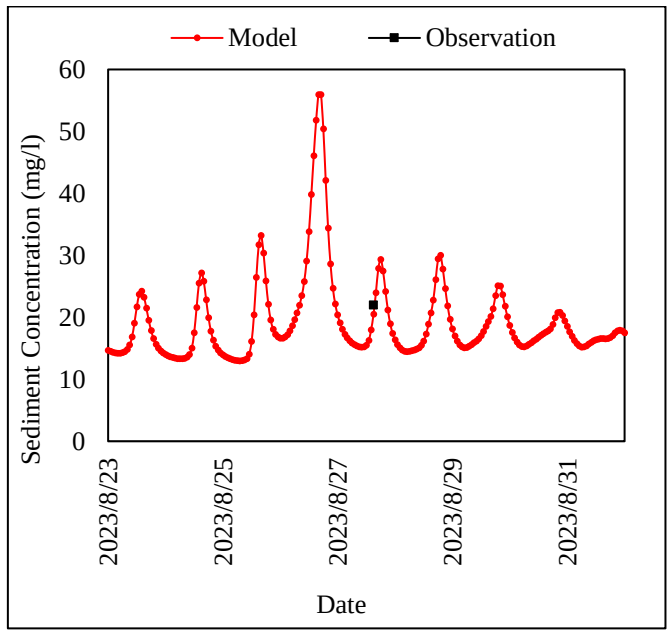

Figure 9. Validation model for SSC at location T7

Figure 9 shows the Suspended Sediment Concentration (SSC) validation result between the model and observation at

T7 Kali Adem Estuary. Figure 10 shows the Suspended Sediment Concentration (SSC) validation result between the model and observation at T8 Kali Adem Estuary. The validation at each site indicates a favorable outcome, with the observed values well aligned with the model.

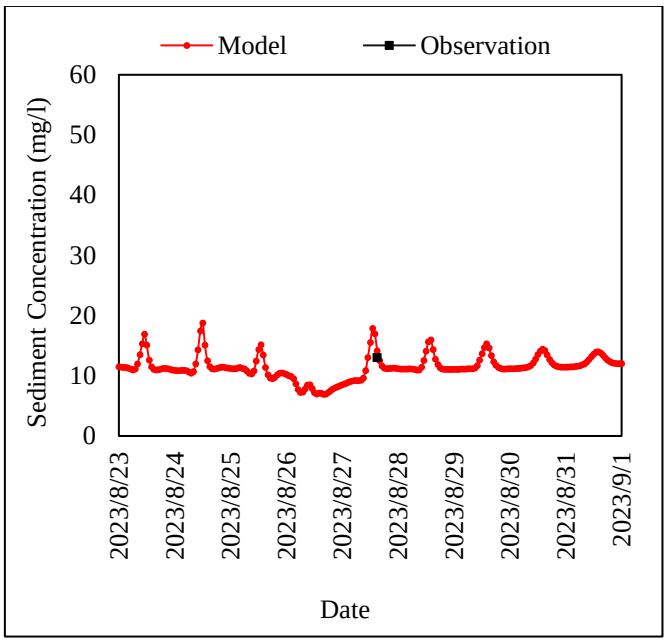

Figure 10. Validation model for SSC at location T8

4.3 Model simulation

This model will for four years for deposition simulation purposes, from Dec 2022 until Dec 2026, using river flow discharge as the key parameter input. The river flow discharge used as model input results from measurements at the PA Karet sluice gate, as seen in Figure 11. The simulation model (Figure 12 and Figure 13) will use the physical parameter for bed friction coefficient is 0.001; erosion rate is 0.2mm/hour; simulation starts from Dec 2022 for four years; physical parameter for sediment settling velocity is 0.8mm/s; critical shear stress for erosion 1.0 Pa; critical shear stress for deposition 0.5 Pa; density sediment 1600Kg.m^{-3}.

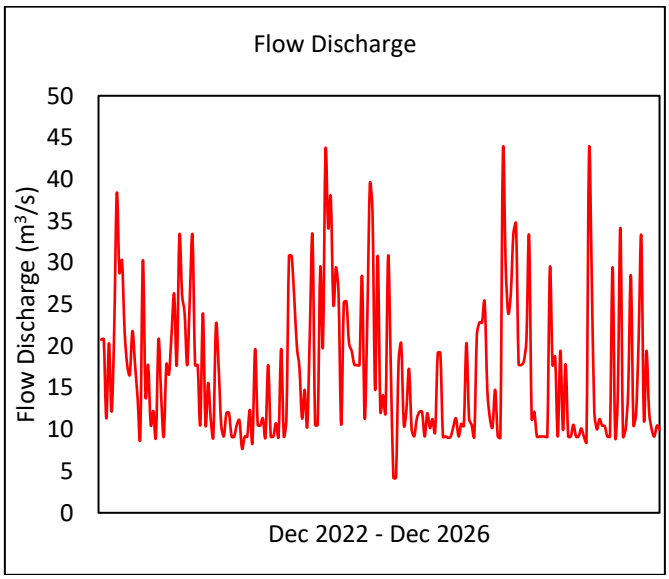

Figure 11. Daily river discharge Dec. 2022 – Dec. 2026

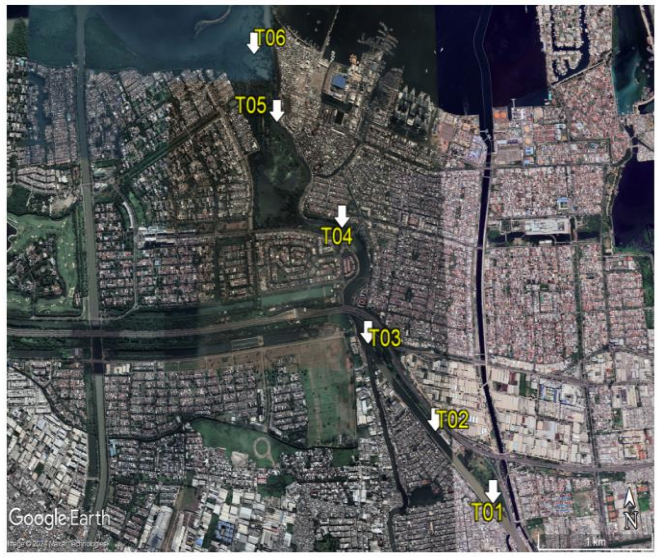

Figure 12. Location for the simulation model (Google Earth)

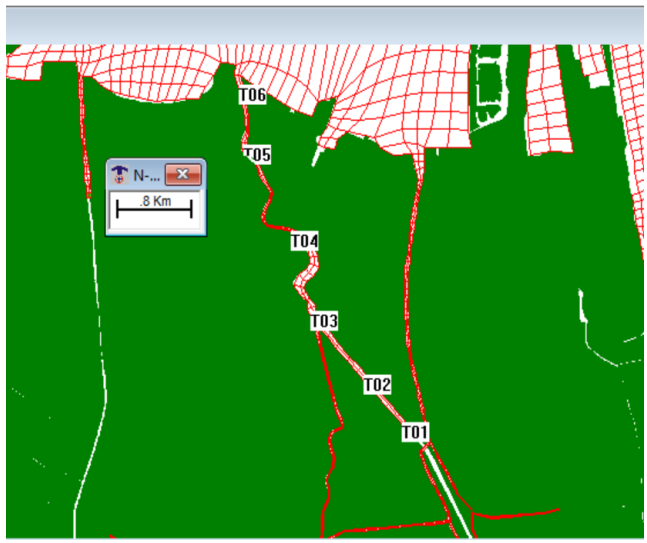

Figure 13. Location for the simulation model (Grid Model)

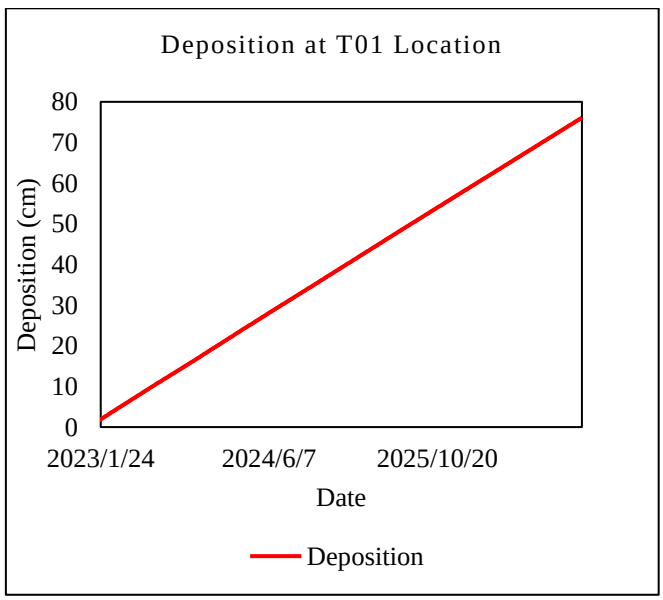

Figure 14. Simulation result time series of deposition at Location T01

The results of the deposition simulations are displayed in Figures 14 until 17.

The model simulation deposition was conducted at six specific locations along the Kanal Banjir Barat as a reference point, as shown in Figure 12 and Figure 13 respectively, for the four-year dry and wet seasons. The result for the time series simulation deposition in sequence based on their location can be seen from Figure 14 until Figure 19. Because of their proximity to the sediment source, sites T01 and T02 in Figure 14 and Figure 15 had the highest result-a 80 cm sediment deposit that occurred over four years. As a result of their distance from the sediment source and the effect of tides on river flow, the sediment deposits at locations T02–T06 are gradually decreasing.

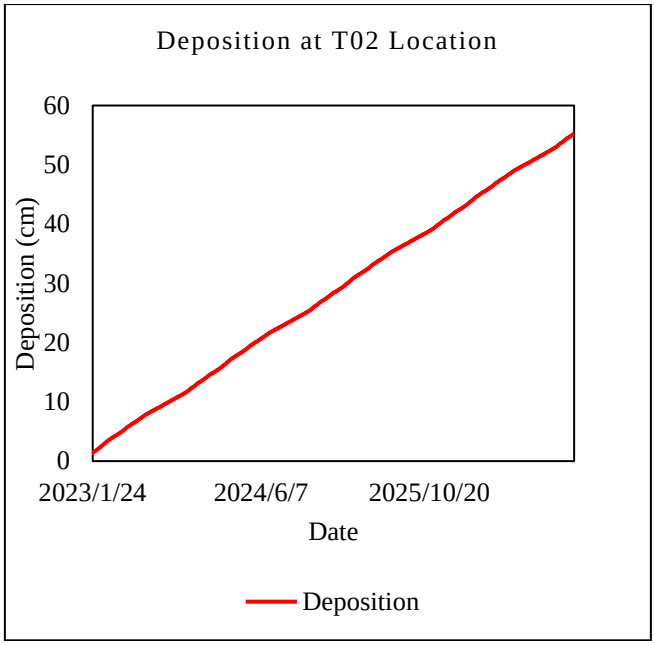

Figure 15. Simulation result time series of deposition at Location T02

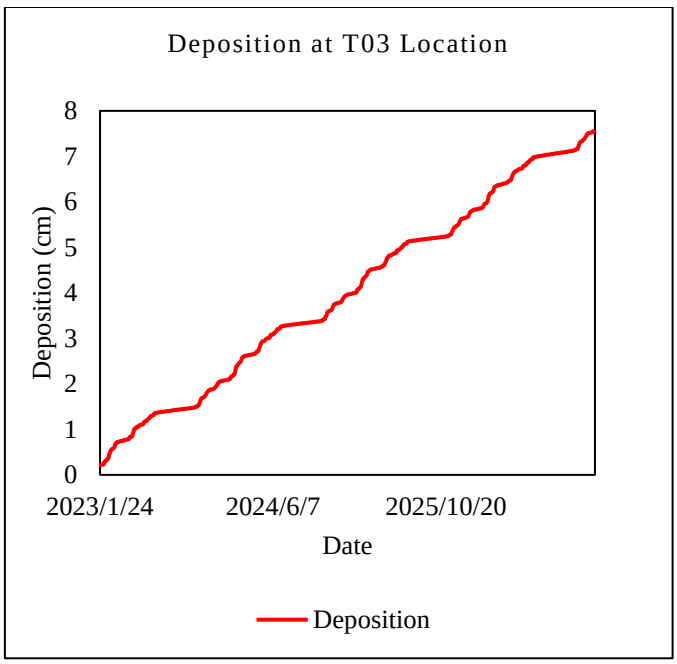

Figure 16. Simulation result time series of deposition at Location T03

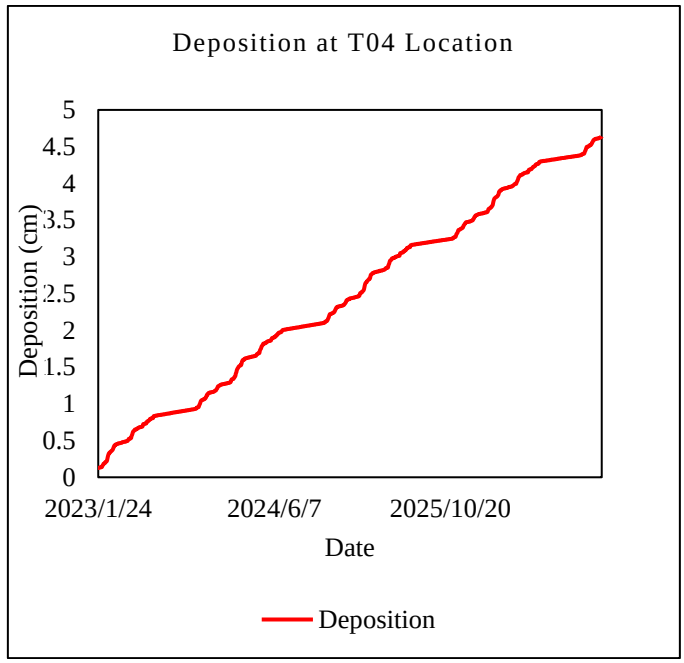

Figure 17. Simulation result time series of deposition at Location T04

Sediment accumulation was seen at the study site according to the contour findings of the yearly model simulation beginning in 2023 and continuing until 2026, as shown in Figure 20. Sediment layers of 55-65cm will be seen in the 2024 simulation in Figure 21, with the heaviest deposits located 3 km away from the Season City Bridge. A 65-70cm thick silt deposit, with a maximum thickness of 3 km along the Season City Bridge, is shown in the 2025 simulation in Figure 22. Figure 23 shows the sediment layers in the 2026 simulation, which are > 70 cm deep; layers as thin as 5 to 10 cm may be observed near the estuary, with the heaviest deposits over a 3-kilometer length from the Season City Bridge.

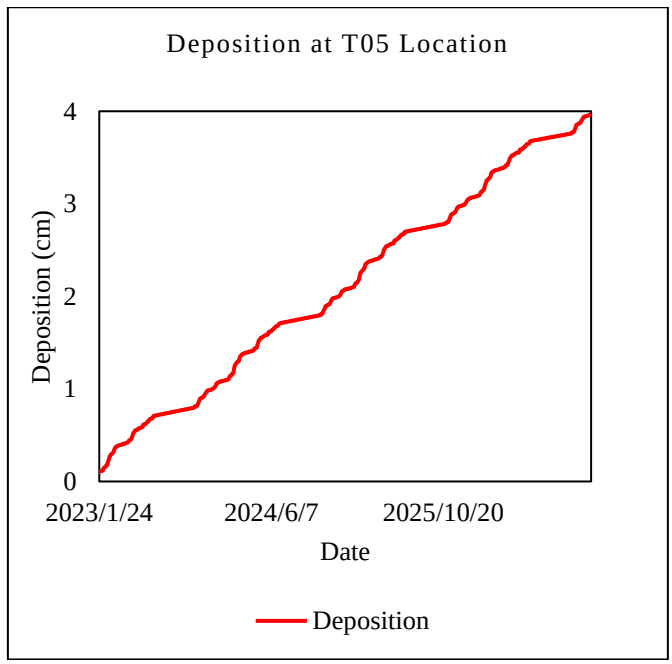

Figure 18. Simulation result time series of deposition at Location T05

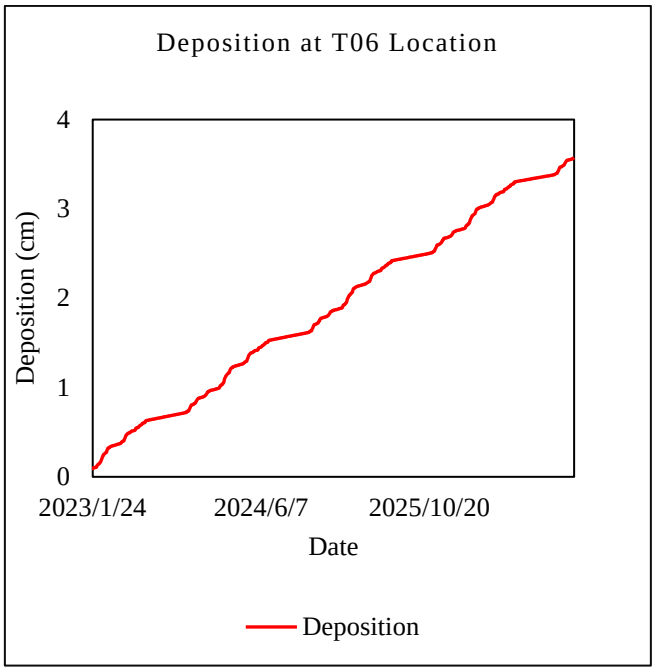

Figure 19. Simulation result time series of deposition at Location T06

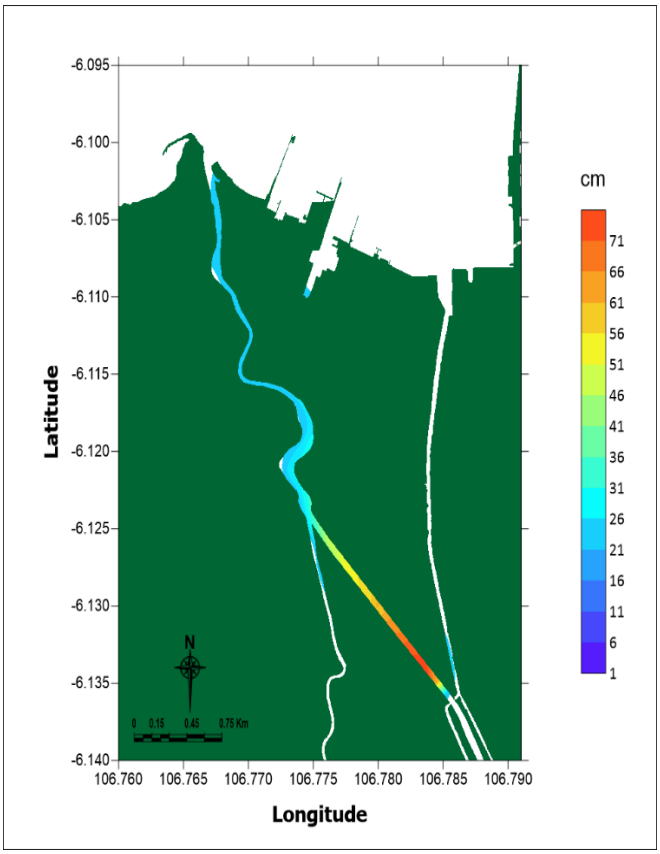

Figure 20. Contour for deposition in 2023

Cohesive sediment transport in rivers can be influenced by a variety of factors, such as advection, dispersion, aggregation, deposition, and consolidation of deposits. Put simply, cohesive sediment is a significant component in the sedimentation process within rivers, specifically in the remote or mixed zone, before its discharge into the sea. As an artificial channel through which river water travels from upstream to downstream of the sea, the Kanal Banjir Barat must be preserved to prevent sedimentation from reducing its width and depth.

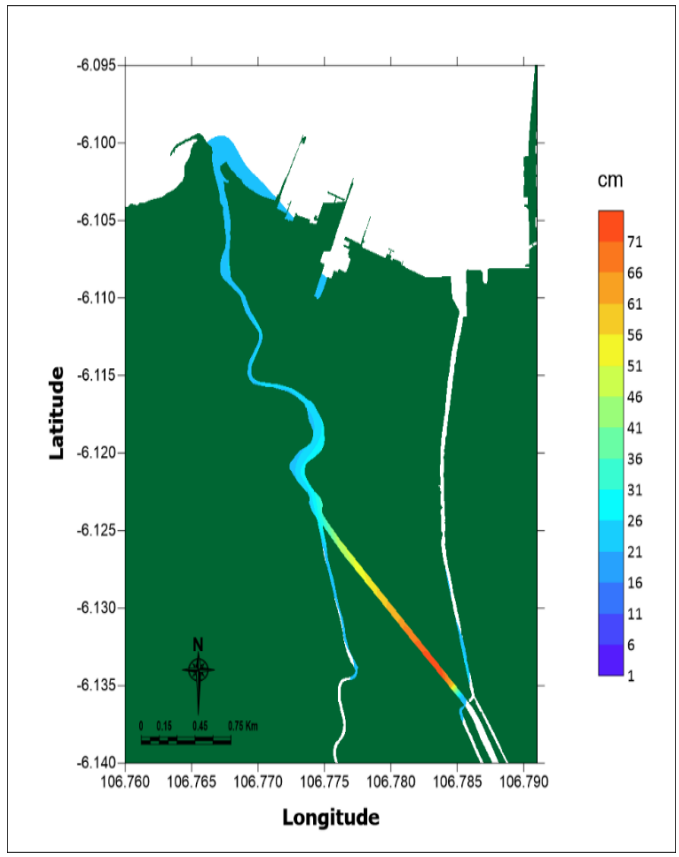

Figure 21. Contour for deposition in 2024

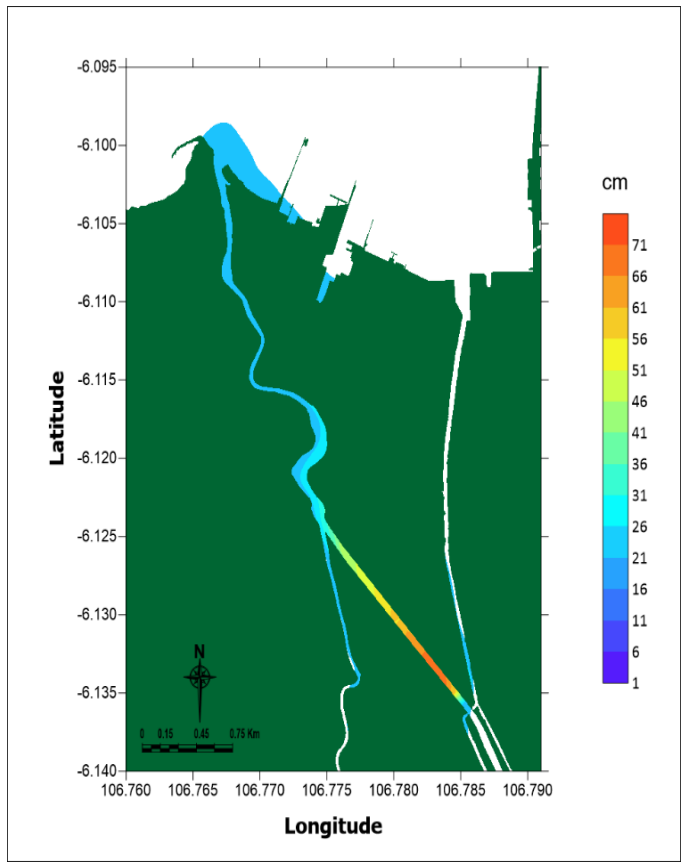

Figure 22. Contour for deposition in 2025

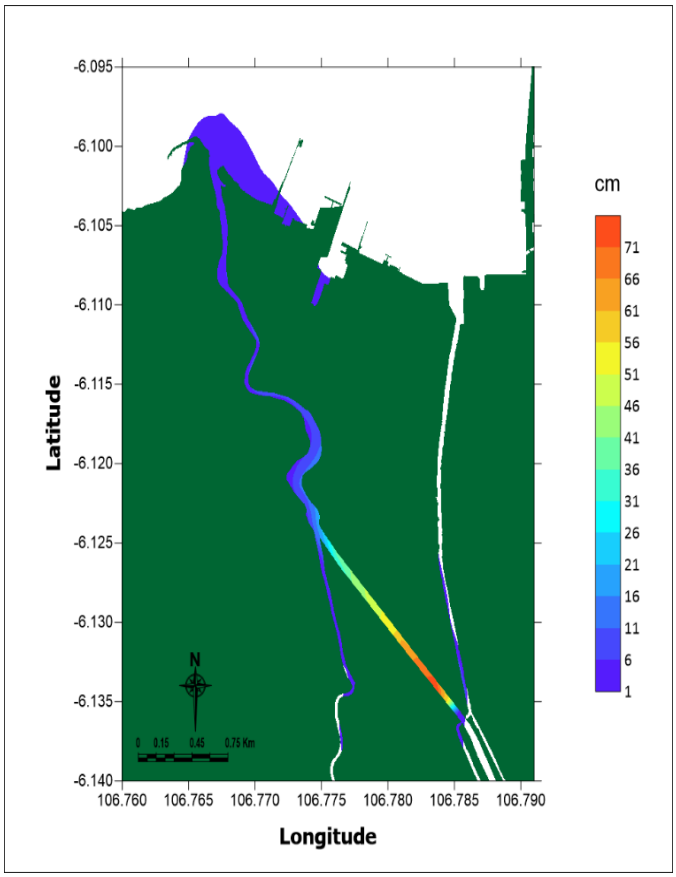

Figure 23. Contour for deposition in 2026

KBB, located downstream in the river, that flows into the estuary, is predominately composed of cohesive, fine-grained sediments transported downstream from their source upland. Density Induced Current in river streams in which seawater infiltrates, current processes facilitate the aggregation of fine-grained cohesive sediments by saltwater, which subsequently settle in specific sections of the river, particularly in the zone where freshwater and saltwater converge due to the transport of seawater during high tides.

The deposition of sediment present in a given section of a river stream significantly impacts the river's downstream flow to the sea. Consequently, it is important to conduct research concerning cohesive sediment movement, with a particular focus on the mixed zone region, where salinity and tides influence sediment deposition; this condition has similarities to other studies investigating the impact of salinity on fine and cohesive sediments [30-33].

5. CONCLUSIONS

Based on the findings from the calibration and validation processes, it is evident that the models align reasonably well with field observation data. Various sediment depositions at the research site locations are produced by model simulations throughout four years, from 2022 to 2026. Sediment thickness decreases from its thickest point in Season City (T01) to its thinnest point at the Kali Adem estuary (T06). In 2026, in a 3-kilometer section of Season City, the biggest silt layer will be more than 70cm.

Consequently, the sediment transport model called MuSed3D was successfully employed as a tool in the prediction of cohesive sediment movement. Furthermore, the model simulation outcome will enhance comprehension of the deposition and resuspension mechanisms involved in cohesive sediment movement within the river which is induced by river flow and density.

Currently, no research has demonstrated any related sedimentation in Kanal Banjir Barat. Previous studies at this research location, Kanal Banjir Barat (KBB), have always concentrated on flooding, not sedimentation, especially cohesive sediments. This study concludes that flooding an area with cohesive sediments can cause sedimentation, affecting the estuary. Based on the findings of the model simulations conducted from 2023 to 2026, it has been shown that the deposit extends up to 3 km from the study location in Season City. In addition, dredging to maintain the canal depth becomes critical if the sedimentation depth blocks the upstream flow of river water.

This study's erosion rate and critical shear stress parameters are based on values from prior researches [23-25]. For further research, additional investigation is required to conduct laboratory experiments to accurately measure critical shear stress and erosion rate, utilizing soil samples obtained from the current study site. Subsequently, a sensitivity analysis is conducted and compared with the findings of previous investigations to figure out the deviation of divergence.

ACKNOWLEDGMENT

The author expresses gratitude to the Laboratory of Civil Engineering at Politeknik Negeri Jakarta and Institut Teknologi Bandung especially Ocean Engineering and Water Engineering Research Group for their support and cooperation.

REFERENCES

[1] ASTM Committee D-18 on Soil and Rock. (2017). Standard practice for classification of soils for engineering purposes (unified soil classification system) 1. ASTM International.

[2] Wan, Y., Wu, H., Roelvink, D., Gu, F. (2015). Experimental study on fall velocity of fine sediment in the Yangtze Estuary, China. Ocean Engineering, 103: 180-187. https://doi.org/10.1016/j.oceaneng.2015.04.076

[3] Isnaeni, M., Kusuma, M.S.B., Nugroho, J. (2021). Comparison of four particle deposition rate formulae in laminar flow. International Journal of GEOMATE, 21(84): 103-111. https://doi.org/10.21660/2021.84.j2160

[4] Lepesqueur, J., Hostache, R., Martínez-Carreras, N., Montargès-Pelletier, E., Hissler, C. (2019). Sediment transport modelling in riverine environments: On the importance of grain-size distribution, sediment density, and suspended sediment concentrations at the upstream boundary. Hydrology and Earth System Sciences, 23(9): 3901-3915. https://doi.org/10.5194/hess-23-3901-2019

[5] Ramalingam, S., Chandra, V. (2019). Experimental investigation of water temperature influence on suspended sediment concentration. Environmental Processes, 6: 511-523. https://doi.org/10.1007/s40710-019-00371-0

[6] Kardhana, H., Valerian, J.R., Rohmat, F.I.W., Kusuma, M.S.B. (2022). Improving Jakarta's katulampa barrage extreme water level prediction using satellite-based long

short-term memory (LSTM) neural networks. Water, 14(9): 1469. https://doi.org/10.3390/w14091469
[7] Yuanita, N., Tingsanchali, T. (2008). Development of a river delta: A case study of Cimanuk river mouth, Indonesia. Hydrological Processes, 22(18): 3785-3801. https://doi.org/10.1002/hyp.6987
[8] Kurniawan, A., Egon, A., Sujatmiko, K.A., Malakani, A.I. (2022). Hydrodynamic modelling of tidally-influenced fluvial zone, A study case of Palembang, Indonesia. ILMU KELAUTAN: Indonesian Journal of Marine Sciences, 27(1): 83-92. https://doi.org/10.14710/ik.ijms.27.1.83-92
[9] Kusuma, M.S.B. (2009). Development study of turbulent κ-ε model for recirculation flow III: Two dimension recirculation flow in a reservoir. Journal of Engineering and Technological Sciences, 41(1): 1-16. https://doi.org/10.5614/itbj.eng.sci.2009.41.1.1
[10] Chen, W.B., Liu, W.C., Hsu, M.H., Hwang, C.C. (2015). Modeling investigation of suspended sediment transport in a tidal estuary using a three-dimensional model. Applied Mathematical Modelling, 39(9): 2570-2586. https://doi.org/10.1016/j.apm.2014.11.006
[11] Dargahi, B. (2004). Three-dimensional flow modelling and sediment transport in the River Klarälven. Earth Surface Processes and Landforms: The Journal of the British Geomorphological Research Group, 29(7): 821-852. https://doi.org/10.1002/esp.1071
[12] Kurniawan, A., Satria, R.A., Pratama, M.B. (2020). Analyzing tsunami hazard using numerical modelling: Study case palu, sulawesi tengah, Indonesia. IOP Conference Series: Materials Science and Engineering, 982(1): 012036. https://doi.org/10.1088/1757-899X/982/1/012036
[13] Luo, J., Luo, Y., Cheng, X., Liu, X., Wang, F., Fang, F., Cao, J., Liu, W., Xu, R. (2023). Prediction of biological nutrients removal in full-scale wastewater treatment plants using H_2O automated machine learning and back propagation artificial neural network model: Optimization and comparison. Bioresource Technology, 390: 129842. https://doi.org/10.1016/j.biortech.2023.129842
[14] Bennett, W.G., Karunarathna, H., Xuan, Y., Kusuma, M.S., Farid, M., Kuntoro, A.A., Rahayu, H.P., Kombaitan, B., Septiadi, D., Kesuma, T.N.A., Haigh, R., Amaratunga, D. (2023). Modelling compound flooding: A case study from Jakarta, Indonesia. Natural Hazards, 118(1): 277-305. https://doi.org/10.1007/s11069-023-06001-1
[15] Muin, M., Spaulding, M. (1997). Three-dimensional boundary-fitted circulation model. Journal of Hydraulic Engineering, 123(1): 2-12. https://doi.org/10.1061/(ASCE)0733-9429(1997)123:1(2)
[16] Muin, M., Spaulding, M. (1996). Two-dimensional boundary-fitted circulation model in spherical coordinates. Journal of Hydraulic Engineering, 122(9): 512-521. https://doi.org/10.1061/(ASCE)0733-9429(1996)122:9(512)
[17] Sankaranarayanan, S., McCay, D.F. (2003). Application of a two-dimensional depth-averaged hydrodynamic tidal model. Ocean Engineering, 30(14): 1807-1832. https://doi.org/10.1016/S0029-8018(03)00014-3
[18] Sankaranarayanan, S., McCay, D.F. (2003). Three-dimensional modeling of tidal circulation in Bay of Fundy. Journal of Waterway, Port, Coastal, and Ocean Engineering, 129(3): 114-123. https://doi.org/10.1061/(ASCE)0733-950X(2003)129:3(114)
[19] Kesuma, T.N.A., Kusuma, M.S.B., Farid, M., Kuntoro, A.A., Rahayu, H.P. (2022). An assessment of flood hazards due to the breach of the manggarai flood gate. GEOMATE Journal, 23(95): 104-111. https://doi.org/10.21660/2022.95.3055
[20] Leendertse, J.J. (1967). Aspects of computational model for long period water wave propagation. Doctoral Disseration. TU Delft.
[21] Swanson, J.C., Spaulding, M., Mathisen, J.P., Jenssen, O.O. (1989). A three dimensional boundary fitted coordinate hydrodynamic model, Part I: development and testing. Dt. Hydrog, (42): 169-186. https://doi.org/10.1007/BF02226293
[22] Muin, M., Spaulding, M. (1997). Application of three-dimensional boundary-fitted circulation model to Providence River. Journal of Hydraulic Engineering, 123(1): 13-20. https://doi.org/10.1061/(ASCE)0733-9429(1997)123:1(13)
[23] Muin, M., Sihombing, R., Hermawan, M.W., Muslim, A.B., Alam, H.N. (2022). Role of non-orthogonal hydrodynamic and sedimentation model for port facilities analysis on port of kuala tanjung. IOP Conference Series: Earth and Environmental Science. IOP Publishing, 1065(1): 012032. https://doi.org/10.1088/1755-1315/1065/1/012032
[24] Muin, M. (2021). Sediment dispersion modeling of a non-orthogonal boundary fitted technique: Mangrove reclamation to protect cliff erosion in bintuni bay, Indonesia. Journal of Coastal Research, 114(SI): 544-548. https://doi.org/10.2112/JCR-SI114-110.1
[25] Muin, M., Karjadi, E.A., Yuanita, N., Ammylia Yusuf, I.Y. (2019). Application of a 3D Non-Orthogonal Ocean Circulation and Sediment Transport Model on Pipeline Risk Assessment due to Dredging Activity in West Java, Indonesia. Journal of Coastal Research, 91(SI): 1-5. https://doi.org/10.2112/SI91-001.1
[26] Muin, M., Idris, K., Yuanita, N. (2016). Application of large-scale 3D non-orthogonal boundary fitted sediment transport model and small-scale approach for offshore structure in Cimanuk Delta North Java Sea. Bandung Institute of Technology. Journal of Engineering Science and Technology, 48(3): 301-319. https://doi.org/10.5614/j.eng.technol.sci.2016.48.3.5
[27] Wang, Y.C., Hung, R.Y. (2023). Effects of sediment properties on the erosion resistance of natural cohesive soils in Taiwan. Catena, 223: 106950. https://doi.org/10.1016/j.catena.2023.106950
[28] Nafchi, R.F., Samadi-Boroujeni, H., Vanani, H.R., Ostad-Ali-Askari, K., Brojeni, M.K. (2021). Laboratory investigation on erosion threshold shear stress of cohesive sediment in Karkheh Dam. Environmental Earth Sciences, 80: 681. https://doi.org/10.1007/s12665-021-09984-x
[29] Pushidrosal. (2024). Indonesian Hydrographic Data Center (IHDC). https://telemetri.pushidrosal.id/enavigation/.
[30] Portela, L.I., Ramos, S., Teixeira, A.T. (2013). Effect of salinity on the settling velocity of fine sediments of a harbour basin. Journal of Coastal Research, 65: 1188-1193. https://doi.org/10.2112/SI65-201.1

[31] Thoman, R.W., Niezgoda, S.L. (2008). Determining erodibility, critical shear stress, and allowable discharge estimates for cohesive channels: Case study in the Powder River basin of Wyoming. Journal of Hydraulic Engineering, 134(12): 1677-1687. https://doi.org/10.1061/(ASCE)0733-9429(2008)134:12(1677)

[32] Beckers, F., Koca, K., Haun, S., Noack, M., Gerbersdorf, S.U., Wieprecht, S. (2022). Functional relationships between critical erosion thresholds of fine reservoir sediments and their sedimentological characteristics. Journal of Hydraulic Engineering, 148(10). https://doi.org/10.1061/(ASCE)HY.1943-7900.0001984

[33] Silva, A.S.R., Noack, M., Schlabing, D., Wieprecht, S. (2018). A data-driven fuzzy approach to simulate the critical shear stress of mixed cohesive/non-cohesive sediments. Journal of Soils and Sediments, 18: 3070-3081. https://doi.org/10.1007/s11368-017-1860-8

NOMENCLATURE

C	sediment concentration, gr/l
S	salinity, ppt
q	concentration of conservative substance such as S or Θ
t	time, second
g	acceleration of gravitation, m/s^2
h	water depth, m
D	water depth+water surface elevation, m
R	earth radius, km
ω	vertical velocity in σ-coordinate, $m.s^{-1}$
ω_s	settling velocity in σ-coordinate, $m.s^{-1}$
τ_s	surface shear stress, Pa
τ_b	bottom shear stress, Pa
S	salinity, ppt
Θ	temperature in centigrade
ξ, η	curvilinear coordinate
ρ	density sediment, $kg.m^{-3}$
μ	dynamic viscosity, kg. $m^{-1}.s^{-1}$
Ω^n	concentration of n-th class of suspended sediment material